Acta Materialia 161 (2018) 54–60

Contents lists available at ScienceDirect

Acta Materialia

journal homepage: www.elsevier.com/locate/actamat

Full length article

Low-temperature intrinsic plasticity in silicon at small scales

A. Merabet [a], M. Texier [a, *], C. Tromas [b], S. Brochard [b], L. Pizzagalli [b], L. Thilly [b], J. Rabier [b], A. Talneau [c], Y.-M. Le Vaillant [d, 1], O. Thomas [a], J. Godet [b]

[a] Aix Marseille Univ, Université de Toulon, CNRS, IM2NP, Marseille, France
[b] Institut Pprime, CNRS, Université de Poitiers, F-86962, Futuroscope Chasseneuil, France
[c] LPN, C2N, Université de Paris Sud, CNRS, Marcoussis, France
[d] Soitec, Chemin des Franques, 38190, Bernin, France

ARTICLE INFO

Article history:
Received 20 June 2018
Received in revised form
13 September 2018
Accepted 13 September 2018
Available online 15 September 2018

Keywords:
Brittle-to-ductile transition
Plasticity
Dislocations
Size effect
Silicon

ABSTRACT

The mechanical properties of materials usually depend on the size of the considered object. Silicon, for instance, undergoes between the macroscopic and nanometer scales, a brittle-to-ductile transition at room temperature. Although essential for the constantly developing Si-based nanotechnologies, the origin of this remarkable behaviour change remains undetermined for several years. The observation of the mechanisms responsible for plastic deformation in nano-objects is indeed highly challenging at the microscopic scale. One needs controlling the deformation while identifying induced individual plastic events at the smallest scale during the first stages of plasticity. This work describes nano-compression experiments on 100 nm-diameter Si nanopillars followed by post-mortem analysis of the deformed specimens through SEM and atomic resolution TEM imaging. The observed plastic deformation disrupts the usual description of low-temperature undissociated-dislocations-mediated plasticity and is comforted by molecular dynamics calculations. These results shed a new light on the transition between ductile and brittle regimes in silicon by introducing the missing link between plasticity and fracture.

1. Introduction

Among all semiconducting materials, silicon occupies a central place as the basic element of the microelectronics industry since more than fifty years. The performance of this material can still be intensively enhanced through various engineering developments such as crystal orientation, strain engineering, nanowire geometry [1]. Because of both its industrial interest and the high control of its crystal growth, which makes silicon a model material for fundamental studies, possible dislocation types in this material have been theoretically investigated since the early 60's [2–4], and its mechanical properties have been widely studied both in ductile and brittle regimes, *i.e.* at high and low temperatures respectively [5]. In particular, for bulk material, the deformation mechanisms above the brittle-to-ductile transition (BDT) temperature (~700K) are highly documented and rely on the propagation of partial dislocations in the {111} close-packed planes of the diamond structure [6,7]. In the brittle regime, plastic deformation induced by compression experiments performed at very high stresses has been attributed to the propagation of non-dissociated dislocations [8,9]. The transition between the two regimes is supposed to be correlated with the respective temperature-and-stress-dependent mobility of either partial or perfect dislocations [10–12]. In addition, recent works revealed a size-dependent BDT temperature in silicon, evidenced by the ductile behaviour of silicon nano-objects deformed at room temperature [13–19]. These observations have thus raised new questions concerning the plasticity at small scale/low temperature in silicon and the origin of the BDT. At the same time, the size effect on BDT has also been observed in other semiconducting materials such as silicon carbide [20], GaAs [21] and InSb [22] or in metallic glasses [23]. These recent studies have highlighted the intriguing mechanical behaviour of semiconducting materials at small scales, while constituting the starting point for fundamental researches [24–26] aiming at elucidating this puzzling issue whose scope is considerable for future applications in the field of nanotechnology.

In this study, silicon nanopillars with small diameters of 100 nm and 340 nm in height have been considered. The <110> crystallographic orientation of the nanopillars allows an easy identification

* Corresponding author.
E-mail address: michael.texier@univ-amu.fr (M. Texier).
[1] Present address: Nelumbo Digital SAS, 143 rue du Brocey, 38920 Crolles, France.

https://doi.org/10.1016/j.actamat.2018.09.025
1359-6454/

of the elementary deformation mechanisms in the ductile regime, since only two equivalent {111} slip systems are activated for such deformation conditions. The post mortem high-resolution transmission electron microscopy (HRTEM) analyses of plastically deformed silicon nanopillars as well as molecular dynamics simulations reveal that the ductile behaviour of these objects involves several types of dislocations whose core equilibrium states exhibit polymorphic configurations. Here, we notably demonstrate the presence of isolated dissociated 60° dislocations, which leads to revisit the paradigm of low temperature plasticity in silicon resting on the propagation of perfect dislocations in the shuffle set [9,27,28]. The confrontation of the experimental results with molecular dynamics (MD) simulations underlines the respective roles of perfect and partial dislocations.

This study allows deeply reinterpreting the experimental data recently reported in the literature and highlights the intricate relationship between BDT, dislocation interactions, and size effect.

2. Experimental details

<110> oriented nanopillars (*cf.* Fig. 1a) have been defined by e-beam lithography and etched by reactive ion etching (RIE) from a <110> oriented silicon-on-insulator (SOI) substrate. A dedicated fluorine-based process has been optimized for vertical and smooth sidewalls without trenching. The whole superficial [110]-oriented silicon layer of silicon-on-insulator (SOI) wafers has been etched. The geometry of the obtained nano-pillars is almost perfectly cylindrical with a negligible superficial roughness and the sole presence of a very thin native oxide layer, as confirmed later by the TEM observations of the pristine nanopillars. Thus, the highly-controlled shape and the quality of the crystal exhibited by the nanopillars elaborated using the RIE process allow to exclude the possible influence of surface defects or superficial irregularities on the deformation mechanisms.

The compression tests were carried out with a nanoindenter U-NHT from Anton Paar, equipped with a diamond flat punch. The misalignment between the flat punch and the pillars was less than 0.4°. The U-NHT design presents an active reference at the contact of the sample surface, which provides a very high mechanical and thermal stability. The force and the displacement were measured with two independent sensors, and the experiments were performed in depth control mode, with a displacement rate of the indenter of 10 nm min^{-1}, which corresponds to a strain rate of 5.4×10^{-4} s^{-1}. The engineering stress was calculated from the applied load and from the diameter at half the pillar height, and the engineering strain was calculated from the measured displacement after correcting the effect of the SiO_2 substrate compliance thanks to the Sneddon's equation [29].

HRTEM imaging was carried out using an aberration corrected FEI Titan 80–300 microscope, operating at 200 kV to reduce the irradiation damaging. Spherical aberration C_s was set to about −10 µm in order to both improve spatial resolution and optimize the phase contrast [30]. Analysis of the post mortem HRTEM images makes use of the comparison between strain mappings extracted from both experimental images and simulated ones. This method allows discerning slightly different dislocations microstructures in case of very closely interacting defects, even if their core structure cannot be thoroughly resolved directly due to the local bending of the TEM lamellae. Thickness of the TEM lamellas was estimated from the comparison between focal series carried out in defect free areas and multislice simulations performed using the JEMS software [31]. The atomic structures used for the image simulations of the deformed areas were built using isotropic calculations obeying the classical elasticity theory [3] and then relaxed with numerical calculations using the Stillinger-Weber semi-empirical potential [32] for refining the atomic positions in the dislocation core regions. Deformation mapping were obtained by geometrical phase analysis [33] of experimental and simulated images using the GPA for DigitalMicrograph plugin from HREM Research Inc. Mapping of the three components ε_{xx}, ε_{yy}, and ε_{xy} of the in-plane strain tensor were extracted from both raw experimental images and simulated images using the geometrical phase analysis (GPA) method described elsewhere [33]. A Gaussian aperture (diameter equals to g/4) was used for the phase reconstruction. In the simulated images, an insert of non-deformed crystal was used as a reference for the strain analysis. Measured

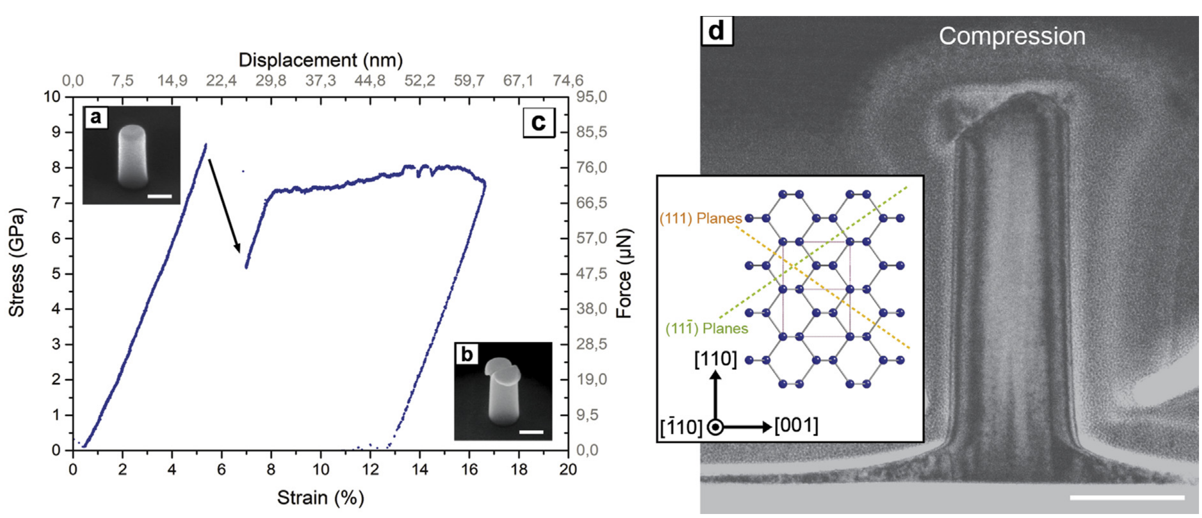

Fig. 1. Plastic deformation of cylindrical silicon nanopillar. **a.** The shape of the pristine nanopillars is cylindrical with a side wall taper of 1.8° (SEM image). **b.** The large shear usually visible at the head of the deformed nanopillars is characteristic of a ductile behaviour. **c.** Experimental deformation curve. Dislocation nucleation events (see black arrow) are evidenced by sudden load drops in the stress-strain curves measured for each deformation experiment. The large plastic flow is characterized by a very slight hardening. A purely elastic response is observed during unloading the sample. **d.** TEM imaging of deformed nanopillars observed in cross section allows to see the localisation of the plastic deformation. It must be noticed that the deformed nanopillar has been embedded in a Pt protective layer before the TEM sample preparation to avoid damaging during the FIB micromachining. The crystallographic orientation of the nanopillar and the silicon crystalline structure are depicted in the inset. The scale bars are 100 nm for both SEM and TEM images. (For interpretation of the references to colour in this figure legend, the reader is referred to the Web version of this article.)

strain is reported in temperature scale on the mappings allowing easily distinguish between the compressive and tensile zones, which form characteristic lobes around edge and mixed dislocations [33]. Stacking faults are evidenced in the strain map by the presence of a trail whose appearance depends on the image defocus. This characteristic footprint results from an artificial calculated strain jump caused by the discontinuity constituted by the stacking fault in the periodic crystalline structure.

The silicon atoms interactions were modeled by the Stillinger-Weber potential that we have optimized in order to get better elastic, plastic and brittle properties [32]. The simulations were done with LAMMPS code [34], in the NVT (canonic) ensemble. The Verlet algorithm was used to calculate atomic trajectories with an integration time step of 1 fs. The temperature (either 10 K or 300 K) was controlled with the Nosé-Hoover thermostat with a small coupling with the thermostat (a temperature damping parameter of 1 ps was used). The deformations were performed at relatively small strain rate of 10^6 s^{-1} compared to usual MD strain rate of 10^8 s^{-1}. As previously proposed by another group [35], this lower strain rate was the key parameter to observe new mechanisms, here dislocation dissociation at low temperature. In Fig. 4, the simulations were done with a set of parameters of the SW potentiel fitted to get the good shear modulus and cell parameter [36]. Atomic configurations were extracted with Ovito [37].

3. Results and discussion

The various stages of deformation (elastic loading, activation of dislocation sources, plastic flow) are distinguishable in the deformation curves extracted from the nano-compression experiments (Fig. 1c). The yield stress value is found to be 8.3 ± 0.8 GPa on average. Large load drops, attributed to massive nucleation events, arise at different stages of the plastic deformation, although the measured force oscillations evidenced during the plastic flow, strongly suggest that continuous nucleation proceeds simultaneously to dislocation multiplication. It must be noticed that, in spite of the high stress values reached during the compression experiments, the phase transformations observed in silicon deformed under hydrostatic pressure [38] or using nano-indentation [39,40] were not evidenced in our deformed nano-pillars. Indeed, the deformation curves do not exhibit the pop-out event characteristic for phase transformations usually observed in

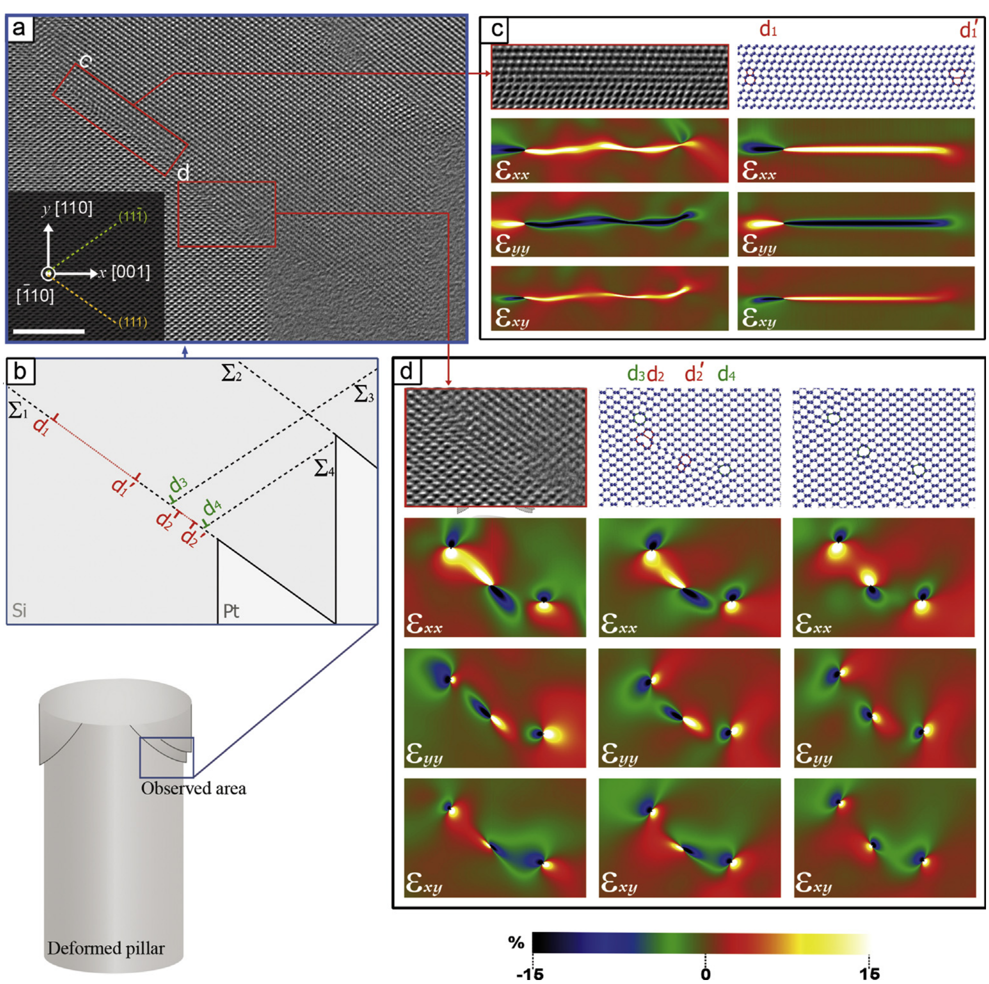

Fig. 2. Perfect and dissociated dislocations. **a.** Experimental image and **b.** schematic description of a sheared zone of the specimen (embedded in the Pt protective layer deposited prior to FIB micromachining). The axis of the nanopillar is vertical. The plastic deformation of this nanopillar ($\varepsilon_{pl} = 5\%$) leads to the formation of a few surface steps visible in the right part of the image, which were produced by the propagation of numerous dislocations in the same slip planes (scale bar 5 nm). **c.** Detail of the experimental image (top-left) and corresponding calculated atomic structure (top-right) containing a dislocation dissociated in a Shockley partial (d_1) and a shuffle partial (d'_1), as suggested by MD observations (Fig. 3f). The strain maps corresponding to the experimental (left) and calculated (right) structures are given below. **d.** Detail of the experimental image (left) and calculated atomic structures constituted by 2 perfect dislocations d_3 and d_4 interacting with a closely dissociated dislocation d_2 and d'_2 (middle) or 3 interacting non-dissociated dislocations (right). The best agreement between strain maps extracted from the experimental image and the calculated structures is obtained with the structure containing the dissociated dislocation.

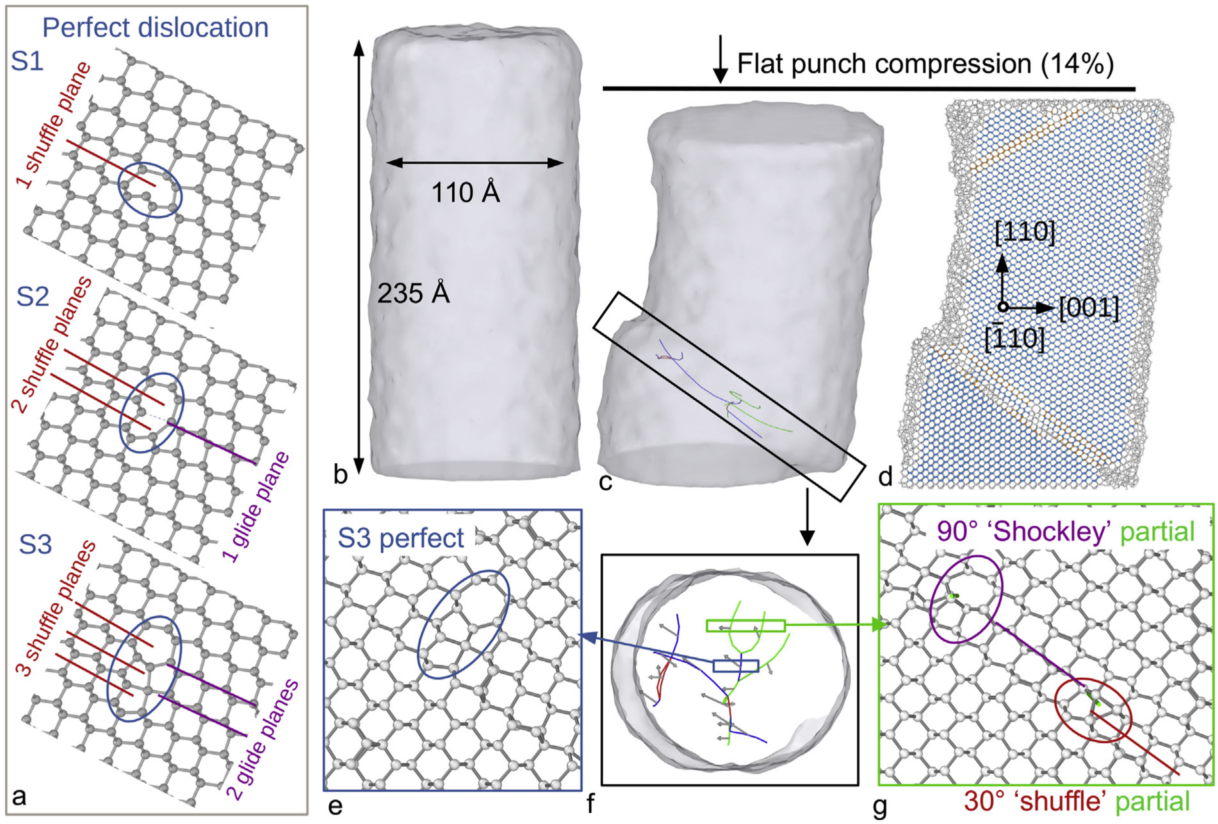

Fig. 3. 300K molecular dynamics simulations of nanopillar compression. **a.** The left panel shows the transient core configuration of a mobile perfect dislocation that is constricted in its slip plane (the shuffle plane) and called S1. When the dislocation stops the core expands on two, then three shuffle planes, the configurations are then called S2 and S3 respectively. In configuration S2 and S3, the dislocation spans onto one or two glide planes (close-packed) and the dislocation cannot move anymore under pure shear stress [28]. **b.** and **c.** 3D mesh reconstruction of the atomic structure before and after compression of 14%. **d.** Slice parallel to the (−1 1 0) plane of the deformed pillar shown in c. Stacking faults are evidenced by orange atoms. **e.** Zoom on txhe atomic structure of the perfect non-dissociated dislocation showing a sessile core S3 expanded on three {111} shuffle planes [28]. f. Slice parallel to the (111) slip plane revealing a perfect dislocation (blue line) that becomes dissociated in two partial dislocations (green lines). The boxes indicate the zoomed zones shown in e. and g. Grey arrows correspond to Burgers vectors. **g.** Zoom on atomic structure of the perfect dislocation after dissociation, revealing composite partial dislocations located in between either the glide-set or the shuffle-set planes, and respectively called 'Shockley' partial dislocation [6,7] and 'shuffle' partial dislocation [30] in the earlier literature. (For interpretation of the references to colour in this figure legend, the reader is referred to the Web version of this article.)

the deformation curves during the elastic unloading of the sample [39] and the post mortem TEM observation only revealed the presence of the Si–I diamond cubic phase. The absence of phase transformations in the deformed nanopillars can be explained by the deconfinement effect proposed by Chrobak et al. [41]. From the post mortem SEM and TEM observations (Fig. 1b and d), we confirm the ductile behaviour of silicon nano-objects at room temperature: the large shearing induced by the uniaxial compression is usually located at the top of the nanopillars during the first stage of deformation, while no crack is visible, except in some nanopillars deformed at the highest strains (ε_{pl}>13%). We notably focused our analyses on the structure of individual extended defects produced in the first stages of deformation, and their interactions while increasing the plastic strain. The nature and core configurations of dislocations were studied using HRTEM imaging and image simulations based on various models of atomic structures of defects, which were built using analytical elasticity equations and relaxed with numerical calculations using the Stillinger-Weber semi-empirical potential [32]. The analysis of the local strain field produced by the various types of defects, measured by the geometrical phase analysis method for the experimental and simulated HRTEM images, was also exploited. This approach allowed us to overcome the limitations of HRTEM imaging for resolving atomic structures, which result from the unavoidable twisting of very thin TEM specimens around structural defects produced under very high stresses. Thanks to this analysis procedure, we were able to unambiguously determine both the type and equilibrium position of isolated and closely interacting defects. Fig. 2 displays HRTEM images and their analyses for relatively low plastic strain (lower than 10%). Fig. 2d reveals the presence of well expected perfect (i.e. non-dissociated) 60° 1/2<1 10>{111} dislocations (d_3 and d_4). The observed configuration implies dislocations gliding in several intersecting slip systems which most probably interact with each other. Indeed, the observed perfect dislocations are likely pinned, as strongly suggested by their equilibrium position, which is located at the intersection of the various activated slip planes (Σ_1, Σ_3 and Σ_4, as shown in Fig. 2b).

More surprisingly, the post mortem analyses of the deformed specimen also indicate the presence of 60° dislocations, which are dissociated into two partial dislocations. The observed dissociated dislocations consist in pairs of partial 1/6<112>{111} dislocations separated by stacking faults extending in the {111} glide set planes (Fig. 2a and b). Using the GPA analysis, we compared the strain mapping extracted from either the experimental HRTEM images, or the simulated HRTEM images of various calculated atomic structures containing different types of dislocations (see Fig. 2c and d). An example of isolated dissociated dislocation is shown in Fig. 2c. This dissociated dislocation consists in a stacking fault, bounded on one side by a 90° (d_1) partial dislocation and on the other side by a 30° (d'_1) partial dislocation, as shown by the excellent agreement

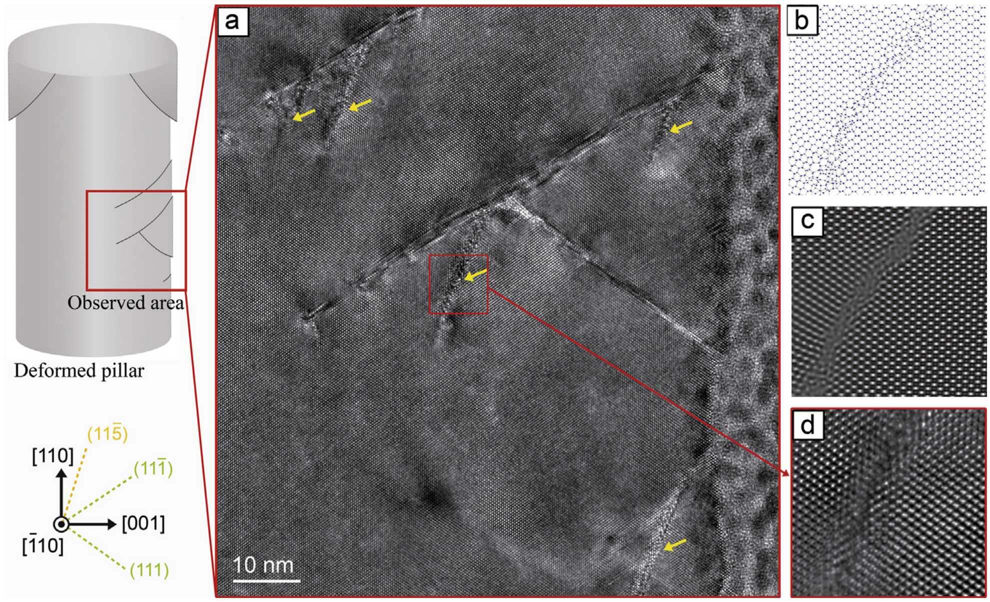

Fig. 4. Transition defects. **a.** HRTEM observation of transition defects observed in nanopillars deformed with the highest values of imposed strain (here $\varepsilon_{pl} = 13\%$). The scale bar corresponds to 10 nm. Plastic events take place in unexpected slip planes (see yellow arrows). This secondary activated system for plastic deformation systematically initiates from pre-activated {111} slip systems. The observed disorder produced by such a transition defect defines corrugated planes, close to the {115} crystallographic planes. **b.** Transition defect obtained by MD calculation performed at 10K. **c.** HRTEM image simulation of the calculated structure shown in b. **d.** Experimental contrast obtained in HRTEM for similar imaging conditions. (For interpretation of the references to colour in this figure legend, the reader is referred to the Web version of this article.)

between experimental and calculated strain maps for the ε_{xx}, ε_{yy} and ε_{xy} components of the strain tensor (Fig. 2c). The stacking fault is evidenced in the strain maps by the presence of a characteristic footprint, which appears as a deformation trail between the two partial dislocation cores. The dissociation length is about 1.7 nm in the strongly interacting configuration (Fig. 2d), whereas this dissociation is only expected at high temperature with a dissociation length about 4–8 nm [42]. Moreover, it appears that the dissociation distance between the leading and the trailing dislocations likely depends on the surrounding microstructure and can reach 8.7 nm in less constrained configuration (Fig. 2c). It must be stressed that dissociated dislocations produced by deformation of silicon were not expected at low temperature and that their direct identification were never reported before in the literature (although partial dislocations and stacking-faults have been suggested in Ref. [16]). To understand the existence of such experimentally observed microstructure, numerical experiments have been performed.

In agreement with experiments, Molecular Dynamics (MD) simulations also evidence the presence of perfect dislocations in the shuffle set, carrying a large part of the plasticity (Fig. 3). As surprisingly as in experiments, under large plastic deformations, 60° dislocations dissociated into two partial dislocations were also observed (Fig. 3f).

A detailed analysis revealed that once the applied stress is exhausted, or under the internal stress caused by plasticity, some of the perfect dislocations stop and their glissile cores (S1 in Fig. 3a) undergo a transformation that spans the core onto 3 slip planes (Fig. 3a,e) decreasing their energy to make them sessile [28]. However, under compressive re-loading, the sessile dislocation (S3) dissociates in one leading Shockley partial dislocation and a trailing partial dislocation, called in early literature 'shuffle partial' [4,43] but never observed until now, respectively located in the glide set plane and in the juxtaposed shuffle set plane (Fig. 3g). This dissociation originates from the dislocation core spanned on several shuffle and glide planes in conjunction with high compressive shear stress that can be sustained by nanopillars. In addition, it appears that the high compressive stress brings the atoms of the consecutive slip planes closer together, such that a flipping mechanism of the atoms in the core region allows the shuffle partial dislocation to glide in its shuffle slip plane, leading to the formation of a stacking fault. Effectively, the shuffle partial dislocation, once nucleated, is quite mobile under 5.5% of shear strain in spite of the low temperature (300K), conversely to the Shockley partial that moves by double kink formation only at high temperature [11] (>700K). Finally, the underrated concept of shuffle partial dislocation appears then as a key defect explaining the formation of stacking faults at low temperature. Then, the propagation of shuffle partial dislocations constitutes the predominant conservative mechanism mainly driven by the high stress sustained by silicon nanostructures, compatible with the well-established scenario of the silicon plasticity at low temperature localized in the shuffle set.

Moreover, to go further in the understanding of the brittle-to-ductile transition, HRTEM images of nanopillars deformed at the highest strain (more than 10%) have been analyzed. Surprisingly, the observations unveiled the formation of straight disordered regions, which spread out along {115} planes (Fig. 4). In addition, these extended defects are systematically nucleated from preliminarily activated {111} slip planes containing a high density of 60° dislocations. Interestingly, this plane orientation was previously found as interphase boundaries between the cubic diamond (3C) and the hexagonal phases (2H) of silicon nucleated during nanoindentation tests [44]. However, the formation of the observed defects is not correlated here with a mechanism involving twin intersections, but likely results from a shear driven mechanism [45], which comes along with phase transformation when thermal activation is efficient [46]. Based on the existence of partial shuffle dislocations and perfect dislocations in strong interaction, one can determine the possible microstructure evolution when increasing the imposed strain, until the fracture of the specimen. Indeed, the dislocation interactions would increase with the imposed strain and the dislocation multiplication should likely favor the various types of mobile dislocations to recombine and form several types of junctions provided the Frank's criterion is satisfied. All the possible reactions between mobile perfect dislocations and partial dislocations resulting from the dissociation of sessile dislocations have in common to produce a shearing out of the {111} dense planes, the slip plane containing both the junction line and Burgers vectors being parallel to either a {112}, a {221} or a {115} crystallographic plane. In addition, the motion of the produced partial junctions should leave a high-energy stacking fault, thus these junctions are assumed to be sessile or weakly mobile leading to strain hardening [47]. Although the nucleation mechanism of these extended defects remains unclear, it is noteworthy that they are consistent with the local shearing associated with the formation of partial locking dislocations through the following reaction:

1/2[101](11-1)+1/6[11-2](111)→ 1/6[411](11-5)

Very similar planar defects were also observed in certain MD simulations (Fig. 4b). The formation of such extended defects may result from the following peculiar conditions: i) interactions between perfect and shuffle partial dislocations gliding in various intersecting {111} slip planes (as shown in Fig. 2), ii) exhaustion of mobile dislocations in the pre-activated {111} slip planes (as shown in Fig. 3), and iii) very high mechanical stresses.

4. Conclusions

This study shows that unexpected deformation mechanisms notably involving shuffle partial dislocations and {115} planar defects, occur in silicon nano-objects submitted to large compressive stress at low temperature.

Several key features are common to the experimental observations and the MD simulations:

- the onset of plasticity is corroborated by the presence of both perfect (non-dissociated) and dissociated dislocations, which were identified by HRTEM imaging in deformed nanopillars as predicted from MD simulations;
- the dissociation of perfect dislocations proceeds at low temperature and leads to the propagation of shuffle partial dislocations and to the formation of stacking faults;
- when increasing the imposed strain, secondary plastic events occur in {115} planes. These extended defects likely result from the recombination of perfect and partial dislocations forming sessile or weakly mobile junctions under large enough stress that can be sustained by the smallest nanostructures which are initially free of cracks and cavities.

The existence of shuffle partial dislocations changes the current picture of plasticity in silicon, notably due to their high mobility and their probable role in the formation of extended stacking faults (already pointed out in nano-objects deformed at low temperature [16]). Furthermore, the defects resulting from the stress concentration out of the {111} slip planes, could constitute the “transition defects” between the ductile and the brittle regimes, possibly inducing the formation and growth of amorphous bands [14,18], or initiating flaws leading to crack nucleation [48]. Thus, the appearance of these defects, unsuspected until now, is proposed to constitute the missing link between the plastic regime governed by the propagation of gliding defects and the brittle regime characterized by the propagation of cracks. Moreover, we believe that the size effect on mechanical behaviour observed in silicon and others semiconducting materials is mainly correlated with the formation of these defects rather than related with surface nucleation of dislocations as proposed by other authors [15,49]. Indeed, the formation of these transition defects likely results from the interaction between various types of mobile dislocations and directly depends on the locking interaction probability. Because of the very high stress levels necessary to nucleate dislocations in an initially defect-free crystal at low temperature, freshly-nucleated dislocations are expected to glide with a high velocity. Thus, only very few dislocations are stored in the smallest nanostructures, which exhibit a high surface-over-volume ratio. The probability for locking dislocation interactions consequently decreases with the decreasing volume of deformed materials and the formation of transition defects, which constitute potential nucleation sites for cracks, is then reduced in nano-objects in comparison with bulk material. Beyond the fundamental scope introduced by the discovery of these original transition defects, this work also underlines the polymorphism of mobile dislocations at low temperature in silicon nanopillars deformed in uniaxial compression which is the mechanical test approaching at best a real nano-device subject to mechanical stress. Among all the various possible dislocation recombinations, some lead to the embrittlement of the material by the formation of transition defects in {115} planes which are potential crack sources. Furthermore, we predict a large sensitivity of the BD transition to the crystal orientation. Indeed, the multiplicity of activated slip systems, hence the crystallographic orientation of the stressed silicon nano-objects, plays an essential role in the ductile-brittle transition at low temperatures. These results bear important consequences on the reliability of nano-electromechanical devices (NEMS) based on Si nanobeams.

Funding sources

We gratefully acknowledge financial support by the French national research agency (ANR) within the project “BrIttle to DUctile transition in silicon at Low dimensions” under the grant reference ANR-12-BS04-0003-01. This work pertains to the French Government program “Investissements d'Avenir” (LABEX INTERACTIFS, reference ANR-11-LABX-0017-01). Computations have been performed on the supercomputer facilities of the Mésocentre de calcul Poitou-Charentes.

References

[1] R.A. Minamisawa, M.J. Süess, R. Spolenak, J. Faist, C. David, J. Gobrecht, K.K. Bourdelle, H. Sigg, Top-down fabricated silicon nanowires under tensile elastic strain up to 4.5%, Nat. Commun. 3 (2012) 1096.
[2] J. Hornstra, Dislocations in the diamond lattice, J. Phys. Chem. Solid. 5 (1958) 129.
[3] J.P. Hirth, J. Lothe, Theory of Dislocations, MacGraw-Hill, New York, 1968.
[4] S. Amelinckx, Dislocations in particular structures, in: F.R.N. Nabarro (Ed.), Dislocations in Solids, vol. 2, North-Holland, 1979, p. 66.
[5] D. Chrobak, N. Tymiak, A. Beaber, O. Ugurlu, W. Gerberich, R. Nowak, Deconfinement leads to changes in the nanoscale plasticity of silicon, Nat. Nanotechnol. 6 (2011) 480.
[6] E. Aerts, P. Delavignette, R. Siems, S. Amelinckx, Stacking fault energy in silicon, J. Appl. Phys. 33 (1962) 3078.
[7] D.J.H. Cockayne, I.L.F. Ray, M.J. Wheelan, Investigations of dislocation strain fields using weak beams, Philos. Mag. A 20 (1969) 1265.
[8] J. Rabier, P. Cordier, T. Tondellier, J.L. Demenet, H. Garem, Dislocation microstructures in Si plastically deformed at RT, J. Phys. Condens. Matter 12 (2000) 10059.
[9] K. Asaoka, T. Umeda, S. Arai, H. Saka, Direct evidence for shuffle dislocations in Si activated by indentations at 77 K, Mater. Sci. Eng. 400–401 (2005) 93.
[10] M.S. Duesbery, Dislocation motion in silicon: the shuffle-glide controversy, Phil. Mag. Lett. 74 (1996) 253.
[11] L. Pizzagalli, P. Beauchamp, Dislocation motion in silicon: the glide-shuffle controversy revisited, Phil. Mag. Lett. 88 (2008) 421.
[12] J. Rabier, L. Pizzagalli, J.L. Demenet, Dislocation in silicon at high stress, in: J.P. Hirth, L. Kubin (Eds.), Dislocations in Solids, vol. 16, North-Holland, 2010 p.47.
[13] F. Östlund, K. Rzepiejewska-Malyska, K. Leifer, L.M. Hale, Y. Tang, R. Ballarini, W.W. Gerberich, J. Michler, Brittle-to-Ductile transition in uniaxial compression of silicon pillars at room temperature, Adv. Funct. Mater. 19 (2009) 2439.
[14] D.-M. Tang, C.-L. Ren, M.-S. Wang, X. Wei, N. Kawamoto, C. Liu, Y. Bando,

M. Mitome, N. Fukata, D. Golberg, Mechanical properties of Si nanowires as revealed by in situ transmission electron microscopy and molecular dynamics simulations, Nano Lett. 12 (2012) 1898.
[15] W. Kang, M. Taher A. Saif, In situ study of size and temperature dependent brittle-to-ductile transition in single crystal silicon, Adv. Funct. Mater. 23 (2013) 713.
[16] A.J. Wagner, E.D. Hintsala, P. Kumar, W.W. Gerberich, K. Andre Mkhoyan, Mechanisms of plasticity in near-theoretical strength sub-100 nm Si nanocubes, Acta Mater. 100 (2015) 256.
[17] L. Wang, D. Kong, T. Xin, X. Shu, K. Zheng, L. Xiao, X. Sha, Y. Lu, Z. Zhang, X. Han, J. Zou, Deformation mechanisms of bent Si nanowires governed by the sign and magnitude of strain, Appl. Phys. Lett. 108 (2016) 151903.
[18] Y.-C. Wang, W. Zhang, L.-Y. Wang, Z. Zhuang, E. Ma, J. Li, Z.-W. Shan, In situ TEM study of deformation-induced crystalline-to-amorphous transition in silicon, NPG Asia Mater. 8 (2016) e291.
[19] Y. He, L. Zhong, F. Fan, C. Wang, T. Zhu, S.X. Mao, In situ observation of shear-driven amorphization in silicon crystals, Nat. Nanotechnol. 11 (2016) 866.
[20] X.D. Han, Y.F. Zhang, K. Zheng, X.N. Zhang, Z. Zhang, Y.J. Hao, X.Y. Guo, J. Yuan, Z.L. Wang, Low-temperature in situ large strain plasticity of ceramic SiC nanowires and its atomic-scale mechanism, Nano Lett. 7 (2007) 452.
[21] F. Öslund, P.R. Howie, R. Ghisleni, S. Korte, K. Leifer, W.J. Clegg, J. Michler, Ductile-brittle transition in micropillar compression of GaAs at room temperature, Phil. Mag. 91 (2011) 1190.
[22] L. Thilly, R. Ghisleni, C. Swistak, J. Michler, In situ deformation of micro-objects as a tool to uncover the micro-mechanisms of the brittle-to-ductile transition in semiconductors: the case of indium antimonide, Phil. Mag. 92 (2012) 3315.
[23] D. Jang, J.R. Greer, Transition from a strong-yet-brittle to a stronger-and-ductile state by size reduction of metallic glasses, Nat. Mater. 9 (2010) 215.
[24] J.D. Nowak, A.R. Beaber, O. Ugurlu, S.L. Girshickd, W.W. Gerberich, Small size strength dependence on dislocation nucleation, Scripta Mater. 62 (2010) 819.
[25] K. Hidashida, M. Tanaka, Mechanism behind brittle-to-ductile transition understood by the interaction between a crack and dislocations, ISIJ Int. 52 (2012) 704.
[26] J.A. El-Awady, Unravelling the physics of size-dependent dislocation-mediated plasticity, Nat. comm. 6 (2015) 5926.
[27] J. Godet, L. Pizzagalli, S. Brochard, P. Beauchamp, Theoretical study of dislocation nucleation from simple surface defects in semiconductors, Phys. Rev. B 70 (2004), 054109.
[28] L. Pizzagalli, J. Godet, S. Brochard, Glissile dislocations with transient cores in silicon, Phys. Rev. Lett. 103 (2009), 065505.
[29] I.N. Sneddon, The relation between load and penetration in the axisymmetric boussinesq problem for a punch of arbitrary profile, Int. J. Eng. Sci. 3 (1965) 47.
[30] M. Texier, J. Thibault-Penisson, Optimum correction conditions for aberration-corrected HRTEM SiC dumbbells chemical imaging, Micron 43 (2012) 516.
[31] P. Stadelmann, EMS – a software package for electron diffraction analysis and HREM image simulation in materials science, Ultramicroscopy 21 (1987) 131.
[32] L. Pizzagalli, J. Godet, J. Guénolé, S. Brochard, E. Holmstrom, K. Nordlund, T. Albaret, A new parametrization of the Stillinger–Weber potential for an improved description of defects and plasticity of silicon, J. Phys. Condens. Matter 25 (2013), 055801.
[33] M.J. Hytch, J.-L. Putaux, J.-M. Penisson, Measurement of the displacement field of dislocations to 0.03 Å by electron microscopy, Nature 423 (2003) 270.
[34] S. Plimpton, Fast parallel algorithms for short-range molecular dynamics, J. Comput. Phys. 117 (1995) 1.
[35] Y. Fan, Y.N. Osetskiy, S. Yip, B. Yildiz, Mapping strain rate dependence of dislocation-defect interactions by atomistic simulations, Proc. Natl. Acad. Sci. Unit. States Am. 44 (2013) 17756.
[36] Private Communication with Tristan Albaret – Lyon.
[37] A. Stukowski, Visualization and analysis of atomistic simulation data with OVITO - the Open Visualization Tool, Model. Simulat. Mater. Sci. Eng. 18 (2010), 015012.
[38] J.Z. Hu, L.D. Merkle, C.S. Menoni, I.L. Spain, Crystal data for high-pressure phases of silicon, Phys. Rev. B 34 (1986) 4679.
[39] V. Domnich, Y. Gogotsi, Effect of phase transformation on the shape of the unloading curve in the nanoindentation of silicon, Appl. Phys. Lett. 76 (2000) 2214.
[40] J.E. Bradby, J.S. Williams, M.V. Swain, In situ electrical characterization of phase transformations in Si during indentation, Phys. Rev. B 67 (2003), 085205.
[41] D. Chrobak, N. Tymiak, A. Beaber, O. Ugurlu, W.W. Gerberich, R. Nowak, Deconfinement leads to changes in the nanoscale plasticity of silicon, Nat. Nanotechnol. 6 (2011) 480.
[42] J.C.H. Spence, H.R. Kolar, G. Hembree, C.J. Humphreys, J. Barnard, R. Datta, C. Koch, F.M. Ross, J.F. Justo, Imaging dislocation cores – the way forward, Phil. Mag. 86 (2006) 4781.
[43] F. Louchet, J. Thibault-Desseaux, Dislocation cores in semiconductors. From the « shuffle or glide » dispute to the « glide and shuffle » partnership, Rev. Phys. Appl. 22 (1987) 207.
[44] P. Pirouz, R. Chaim, U. Dahmen, K.H. Westmacott, The martensitic transformation in silicon - I experimental observations, Acta Metall. Mater. 38 (1990) 313.
[45] T.Y. Tan, H. Föll, S.M. Hu, On the diamond-cubic to hexagonal phase transformation in silicon, Philos. Mag. A 44 (1981) 127.
[46] L. Vincent, D. Djomani, M. Fakfakh, C. Renard, B. Belier, D. Bouchier, G. Patriarche, Shear-driven phase transformation in silicon nanowires, Nanotechnology 29 (2018) 125601.
[47] V. Bulatov, L. Hsiung, M. Tang, A. Arsenlis, M.C. Bartelt, W. Cai, J.N. Florando, M. Hiratani, M. Rhee, G. Hommes, T.G. Pierce, T.D. de la Rubia, Dislocation multi-junctions and strain hardening, Nature 440 (2006) 1174.
[48] F.A. El Nabi, J. Godet, S. Brochard, L. Pizzagalli, Onset of ductility and brittleness in silicon nanowires mediated by dislocation nucleation, Model. Simulat. Mater. Sci. Eng. 23 (2015), 025010.
[49] K. Kang, W. Cai, Size and temperature effects on the fracture mechanisms of silicon nanowires: molecular dynamics simulations, Int. J. Plast. 26 (2010) 1387.